Chemical Engineering Journal 172 (2011) 219–229

Contents lists available at ScienceDirect

Chemical Engineering Journal

journal homepage: www.elsevier.com/locate/cej

Ceria associated manganese oxide nanoparticles: Synthesis, characterization and arsenic(V) sorption behavior

Kaushik Gupta [a], Sayan Bhattacharya [b], Dhrubajyoti Chattopadhyay [c], Aniruddha Mukhopadhyay [b], Harishankar Biswas [d], Jagannath Dutta [d], Nihar Ranjan Ray [d], Uday Chand Ghosh [a,*]

[a] Department of Chemistry, Presidency University (Formerly Presidency College), Kolkata 700073, India
[b] Department of Environmental Science, University of Calcutta, 51/2, Hazra Road, Kolkata 700019, India
[c] B.C. Guha Centre for Genetic Engineering and Biotechnology, 35 Ballygunge Circular Road, Kolkata 700019, India
[d] Saha Institute of Nuclear Physics, Bidhannagore, Salt Lake City, India

ARTICLE INFO

Article history:
Received 26 February 2011
Received in revised form 24 May 2011
Accepted 24 May 2011

Keywords:
Arsenic(V)
Nanoparticle
Ceria associated manganese oxide
Characterizations
Sorption
Synthesis

ABSTRACT

Four samples of ceria incorporated manganese oxide (NCMO) were prepared by co-precipitation-calcinations and sol–gel methods, and characterized by X-ray diffraction, scanning electron microscopy, transmission electron microscopy, atomic force microscopy, BET surface area etc. The synthetic samples were nanoparticle agglomerates with irregular surface morphology (Ce:Mn = 1:1). The NCMO-1b sample, prepared by the calcination of metal hydroxide at 573 K for 3.0 h, was a nano-crystalline (70–90 nm) and hydrated material having high BET surface area (116.96 $m^2 g^{-1}$). The arsenic(V)-sorption by the samples at pH 7.0 (±0.2) and 30 °C showed that the NCMO-1b is a most efficient material. Optimum pH range for the arsenic(V) sorption is 3.0–7.0 at 303 (±1.0) K. Kinetics and equilibrium data obtained (pH = 7.0 ± 0.2, T = 303 ± 1.0 K and I = 0.01 M) had described the pseudo-second order kinetics and the Freundlich isotherm models well, respectively. Thermodynamics of the sorption reaction showed that the changes of enthalpy (ΔH°), entropy (ΔS°) and Gibbs free energy (ΔG°), respectively, were +23.901 kJ mol^{-1}, +0.175 kJ mol^{-1} K^{-1} and −25.737 to −32.753 kJ mol^{-1} at T = 283–323 K. Estimation of the sorption energy (E = 17.15 kJ mol^{-1}) indicated that the arsenic(V) was chemisorbed on NCMO-1b. The phosphate only reduced the arsenic(V) removal efficiency of NCMO-1b.

1. Introduction

Nanomaterials show various unique enhanced properties, which are not shown by the bulk materials, and find their application in multivariate technological fields. Materials with nanostructure have gained special attention recently in the field of solute adsorption from the liquid phase due to the small particle size, large surface area, and high in situ reactivity. Nanomaterials can be used as catalyst to react with toxic gases such as CO and NO_X in automobile catalytic converter for the enhanced chemical activity. Zhang reported an overview of nano-scale iron particles for the environmental remediation [1]. Consequently, different workers [2–6] had adopted the methods such as chemical precipitation, sol–gel, vapor deposition, solvo thermal, solid state reaction, etc. for the synthesis of some mixed oxides. Among the above, the chemical precipitation method is a simple, easy to handle, cheap and mostly green technique. Like different metal oxides with nanostructure, multi metal or doped metal oxides are also to be important for multivariate applications due to the lattice imperfections. However, the simultaneous metal hydroxide precipitate formation from an aqueous mixture containing a number of metal ions is somewhat difficult due to their differences of solubility product values and crystal structures. However, it can be manipulated by controlling the concentrations of metal ions in solution and pH for the precipitation. The difficulty encountered when nano-materials are used for the treatment of contaminated water is the separation of material from its colloidal suspension by simple filtration, but the advantage is the generation of low sludge volume which diminishes disposal problem. However, the difficulty could be overcome by using nano-particle agglomerates of the materials.

The occurrence of arsenic (+3 and +5), which is a carcinogenic element in groundwater much exceeding the tolerance limit (10 μg L^{-1}) is a well known global problem, and poses an ever-increasing degree of health hazard. The Bengal Delta Basin (West Bengal in India and Bangladesh) has become infested with this menace, and in some pockets of this region it has assumed life-threatening, causing deaths of a good number of inhabitants because rural people of those areas are still consuming groundwater as the source of drinking water. Therefore, the removal excess

* Corresponding author at: Department of Chemistry, Presidency University (Formerly Presidency College), kolkata-700073, India. Tel.: +91 33 2241 3893.
E-mail address: ucghosh@yahoo.co.in (U.C. Ghosh).

1385-8947/$ – see front matter © 2011 Elsevier B.V. All rights reserved.
doi:10.1016/j.cej.2011.05.092

arsenic from the contaminated ground water is an urgent need. Among the available different technologies, adsorption is the best one due to its easy handling, high efficiency, and way to develop a filter for house hold purpose.

All these encouraged the workers to synthesis nanoparticle agglomerates of mixed oxides such as iron–cerium [7], iron–manganese [8–11] iron–zirconium [12], iron–titanium [13] and iron–chromium [14] for the arsenic sorption from aqueous solutions. Literatures showed that the synthesis of cerium–manganese mixed oxide had gained special attention for a number of applications such as cerium incorporated porous manganese oxide OMS-2 as catalyst [15], cerium–manganese mixed oxide for the removal of H_2S at high temperature [16], MnO_x-CeO_2 mixed oxide for complete catalytic oxidation of formaldehyde [17], Mn(III)/(IV)-cerium(IV) oxide [18], cerium–manganese mixed oxides as oxidation catalysis [19], etc. Multiple activities of this mixed oxide [15–26] had encouraged us in taking attempt to synthesis cerium–manganese mixed oxide of nano-dimension for scavenging undesired solutes such as arsenic and fluoride from the contaminated groundwater.

This manuscript reports herein the synthesis and characterization of nano-structured ceria associated manganese oxide (NCMO-1 and NCMO-2) samples with arsenic(V) sorption behavior from the aqueous solution.

2. Experimental

2.1. Chemicals

Ammonium ceric nitrate (ACN), manganous chloride, sodium bicarbonate, tartaric acid used for synthesis of the NCMO samples were laboratory reagent (LR) grade, which were procured from E. Merck, Mumbai (India). Disodium hydrogen arsenate (99.99%), which was used for the preparation of stock arsenic(V) solution, was Analar Reagent (A. R.) grade (BDH, England). Sodium chloride used for the ionic strength adjustment was A. R (BDH, England) grade. All other chemicals used were of LR grade (E. Merck, Mumbai, India).

2.2. Synthesis of NCMO-1 samples

The solutions of ACN (0.1 M in 0.1 M HNO_3) and manganous chloride (0.1 M in 0.01 M HCl) were warmed separately at 80 °C. Hot ACN solution was dropped from a separatory funnel slowly into an equal volume of agitating (speed: 300 rpm) hot manganous chloride. To the above agitating mixture, 0.1 M $NaHCO_3$ solution was dropped from the separating funnel till the solution pH rose to ~8.0. The precipitate including mother liquid was kept for 24 h at room temperature for aging. After filtering the precipitate, jell-like mass was washed with distilled water to make carbonate free and dried at 50–60 °C inside an air oven. Dry solid mass was divided into the three fractions, and incinerated for 3.0 h separately at 373, 573 and 773 K which were marked as NCMO-1a, NCMO-1b and NCMO-1c samples, respectively. In addition, manganese oxide and cerium oxide samples were also separately prepared. Here, 0.1 M manganous chloride solution was hydrolyzed with 0.1 M sodium bicarbonate. The basic metal carbonate obtained was ignited at 773 K inside a muffle furnace for 3.0 h for the manganese oxide. The pure ceria was also prepared by cerium oxalate precipitation from 0.1 M ACN solution with 0.1 M oxalic acid. The cerium oxalate precipitate was ignited at 773 K inside a muffle furnace for the cerium oxide for 3.0 h.

2.3. Synthesis of NCMO-2

The NCMO-2 sample was prepared by the sol–gel method. Here, 0.1 M ACN and 0.1 M manganous chloride (1:1, v/v) were mixed together. To this mixture, tartaric acid was mixed (10 times in mole proportion) with mechanical stirring, and placed on a boiling water bath for slow evaporation. The yellow gel formed was calcined at 773 K for 6 h. Here, the gel was converted to grey powder via floppy mass with black color, which was washed with distilled water and dried.

2.4. Analytical tools used for characterizations of NCMO samples

X-ray diffraction (XRD) patterns of the samples were taken by an X-ray powder diffractometer (Philips Analytical PW-1710) with Cu Kα radiation. The potential current and voltage applied were 30 mA and 40 kV, respectively. Atomic Force Microscopic (AFM) images for surface topography of the samples were taken in non-contact mode by multimode scanning probe microscope (Agilent AFM 5500 series, USA) having multi purpose small scanner with low coherence laser (1 mW power, 670 nm wavelength, coherence length (<50 μm), scan range: XY: 0–10 μm; Z: 0–2 μm, noise level: XY < 0.1 nm RMS, Z < 0.02 nm RMS). Föurier Transform Infrared (FTIR) spectra of the mixed oxide samples and the pure oxides were recorded using Perkin Elmer (U.S.) system 2000 spectrophotometer with a resolution of 2 cm^{-1}. Transmission electron micrographic (TEM) images were recorded on a H800 transmission electron micrograph (Hitachi, Japan) operating at 200 kV. Scanning electron microscopic (SEM) images with EDS (Tescan Vega, U.K.; model LSU+) spectra were recorded spraying the sample on a carbon tape. The surface area and pore width distributions were analyzed by Quatachrome Autosorb-1C surface analyzer. The pH of each solution was analyzed by pH-meter of model: LI-127 (ELICO, India).

2.5. Arsenic analysis

Arsenic samples were analyzed using atomic absorption spectrophotometer with hydride generator assembly attachment (Perkin Elmer AAnalyst 200) and UV-VIS spectrophotometer (Hitachi model U-3210) using the methods described in 'Standard Methods for the Examination of Water and Wastewater' [27].

2.6. Arsenic(V) solutions

2.08 g of Na_2HAsO_4 (99.99%) was dissolved in 1.0 L of arsenic free distilled water. The concentration of arsenic(V) was found to be 1000 (±1) mg L^{-1}. Arsenic(V) solution of any desired concentration to be used in the experiments was made by diluting the stock with 0.2% (v/v) HCl. Each arsenic(V) solution was analyzed for the concentration [27] before using in the experiments. The stock solution was prepared fresh after every 15 days.

2.7. Batch experiments

2.7.1. Effect of pH

For the effect of initial pH (pH_i), 50 mg of NCMO was mixed with 50 mL of arsenic(V) solutions of C_0 (initial concentration, mg L^{-1} = 5.0 and 10.0) with ionic strength (I) = 0.01 M and pH_i adjusted separately at 3.0, 4.0, 5.0, 6.0, 7.0, 8.0, 9.0, 10.0 and 11.0 separately into polyethylene tetra phthalate (PET) bottles (each capacity = 250 mL), agitated (speed, S_T = 280 ± 5 rpm) for a duration of 2.0 h at temperature (T) = 300 (±1) K. The equilibrium solution pH (pH_f) value of each mixture was recorded immediately after 2 h of agitation and centrifuged to separate the solid NCMO particles. Each centrifuged solution was analyzed [27] for the remaining arsenic concentration (C_R, mg L^{-1}).

2.7.2. Sorption kinetics

Experiment for the kinetics of arsenic(V) sorption by NCMO at $pH_i = 7.0$ (±0.2), $I = 0.01$ M and $T = 303$ (±1.0) K was carried out by batch method. Here, 500 mL arsenic(V) solution of $C_0 = 10.8$ or 20.0 mg L^{-1} was taken with 0.5 g NCMO into a 1.0 L glass vessel, and placed into a thermostat bath to attain at a desired T (K). It was agitated at $S_T = 280$ (±5 rpm) using a speed adjustable agitator with monitoring of pH. Any major pH change, if any, was re-adjusted to ~7.0 using 0.1 M NaOH or 0.1 M HCl. An exactly known volume of the reaction mixture (2.0 mL at first three stages and 5.0 mL in later stages) was sampled at a definite time interval until equilibrium reached. The sample solutions were centrifuged, and analyzed for the C_R of arsenic [27].

2.7.3. Sorption isotherm

For equilibrium isotherm, experiments were conducted by batch method at $T = 303$ (±1.0) K, $pH_i = 7.0$ (±0.2) and $I = 0.01$ M. Here, 50 mL arsenic(V) solution of C_0 ranged in (5.0–50.0) mg L^{-1} was mixed with 50 mg of NCMO in PET bottles, and agitated $S_T = 280$ (±5) rpm for a duration of 2.0 h. The pH of each reaction mixture was adjusted at $t = 1.0$–1.5 h of agitations from the start of reaction using 0.1 M HCl and/or 0.1 M NaOH, as required. Just after the 2.0 h of agitation, the reaction mixtures were centrifuged for separating NCMO particles, and analyzed for C_R of arsenic in centrifuged samples [27].

2.7.4. Arsenic(V) desorption

Arsenic(V) desorption efficiency of NaOH and KOH solution was investigated by agitation (280–290 rpm) of 50 mL alkali solution (concentration: 0.01–1.0 M) with 25.0 mg As^V-NCMO-1b (27.98 mg As g^{-1}) for a duration of 2 h at $T = 303$ K. Separating the solid particles by centrifugation, arsenic (total) concentration was analyzed in liquid.

2.7.5. Toxicity characteristic leaching procedure (TCLP) test

The TCLP test of As^V-NCMO-1b solid material (27.98 mg As g^{-1}) was carried out according to the procedure described by U.S. EPA method-1311 [28]. Here, the dry arsenic(V)-NCMO-1b material was mixed with the TCLP fluid (sodium acetate plus acetic acid buffer of pH 4.93 (±0.05)) by the 1:20 ratio and agitated (speed, 280 ± 5 rpm) for a duration of 18 h at $T = 303$ K using a mechanical shaker. Leached arsenic in the centrifuged TCLP fluid was analyzed.

3. Results and discussion

3.1. Aims and strategy of the synthetic route

The NCMO-1 sample was prepared by the redox assisted-chemical precipitation reaction. Here, the conversion of $Ce^{4+} \rightarrow Ce^{3+}$ and $Mn^{2+} \rightarrow Mn^{3+}$ took place when hot ACN (0.1 M in 0.1 M HNO_3) was mixed to the hot manganous chloride (0.1 M in 0.01 M HCl). This conversion, $Ce^{4+} + Mn^{2+} \rightarrow Ce^{3+} + Mn^{3+}$, is thermodynamically favorable as the standard reduction potential (E°) values of Ce^{4+}/Ce^{3+} and Mn^{3+}/Mn^{2+} systems are +1.72 V and +1.56 V, respectively, in acid medium and room temperature. Thus, the reduced and oxidized species of metals precipitated simultaneously as hydroxide when the solution pH was increased to 8.0 by adding sodium bicarbonate solution. The gel-like metal hydroxide precipitates obtained for the tri positive metals would now involve in another redox assisted conversion. As E° value for the $Ce^{3+} + 4OH^- \rightarrow CeO_2 + 2H_2O + e^-$ is −0.26 V, and that for the $O_2 + 2H_2O + 4e^- \rightarrow 4\ OH^-$ at slight alkaline pH (8.0) is +0.80 V; the cerium(III) hydroxide should oxidize to cerium(IV) hydroxide in aging period by the aerial oxygen, which went to mixing in molecular level with the manganese(III) hydroxide. Drying the mixed hydroxide precipitate inside an air-oven at 50–60 °C, it was divided into three fractions, and calcined separately at 373 K, 573 K and 773 K for duration of 3.0 h, which were marked as NCMO-1a, NCMO-1b and NCMO-1c samples, respectively.

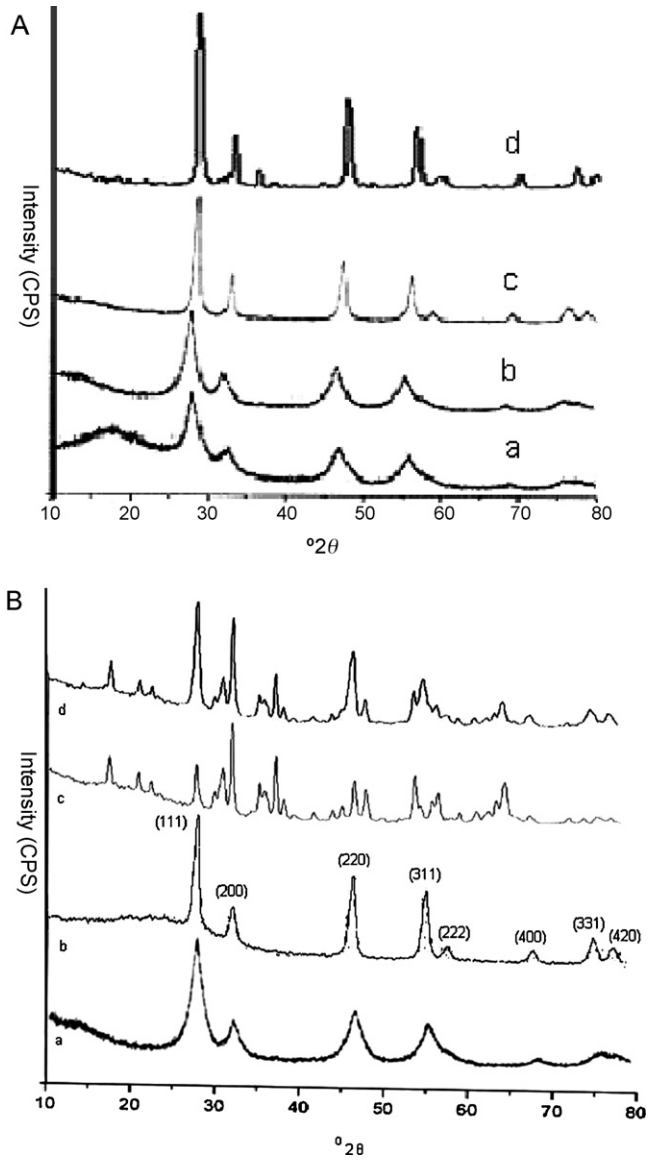

Fig. 1. (A) X-ray diffraction patterns of (a) NCMO-1b, (b) pure CeO_2, (c) pure manganese oxide, and (d) physical mixture of cerium oxide-manganese oxide (1:1). (B) X-ray diffraction patterns of NCMO samples.

In sol–gel method, tartaric acid was used as a complex agent, which should associate with the metal ions with complex formation. The reaction mixture was evaporated slowly on a hot plate to convert into a gum-like gel, and calcined at 773 K for duration of 6.0 h inside a muffle furnace. It was desiccated for cooling to room temperature, and marked as NCMO-2 sample.

3.2. XRD analysis

Fig. 1A shows the XRD patterns for the NCMO samples. The peak patterns indicated that the materials were crystalline. The increase of peak sharpness of the samples from the NCMO-1a (pattern-a) to NCMO-1c (pattern-c) suggested that the crystallites size of the NCMO particles increased with the increase of incineration temperature. Calculations of the crystallites size inserting the XRD data into the Scherer's equation indicated that dimensions (nm) of the crystallites of NCMO-1a, NCMO-1b and NCMO-1c samples

were approximately 60–70, 80–90, and 100–120, respectively. The XRD pattern-d for the NCMO-2 sample suggested the presence of good crystalline cubic phase in the sample. The crystallites size as-calculated by the Scherer's equation from the XRD data showed that the NCMO-2 crystallites had particle size of about 15 nm.

Fig. 1B shows XRD patterns of NCMO-1b (pattern-a), cerium oxide (pattern-b) and manganese oxide (pattern-c) and physical mixture of two pure oxides (pattern-d). It was found that the synthetic oxide (NCMO-1b) is not a simple physical mixture of two pure oxides since the physical mixture of two pure oxides (1:1) showed different XRD patterns and the position of peaks (pattern-d) from the synthetic mixed oxide (pattern-a) (Fig. 1B). Again, the XRD pattern found for the physical mixture of two oxides (pattern-d, Fig. 1B) showed that all the peaks were almost common with those of the pure oxides. The XRD pattern shown for the NCMO-1 (a–c) samples (Fig. 1A) were found to be similar with that for the pure CeO_2 sample (pattern-b, Fig. 1B). The XRD peak at $2\theta = 27.9^\circ$, 46.9°, 55.8°, respectively, with the value of d-spacing = 3.19, 1.94 and 1.65 of cerium oxide (pattern-b, Fig. 1B) could be assigned to the anti fluorite structure of CeO_2 [29]. Again, the XRD peaks at 2θ values = 32.45°, 37.66°, 55.34°, 65.57° for the pure manganese oxide (pattern-c, Fig. 1B) were identical with that of Mn_2O_3 (JCPD file 89-2809). However, the XRD pattern of all the NCMO samples (Fig. 1A) had very little similarity with that of Mn_2O_3, but the position of each diffraction peak was too close with that of CeO_2 [29]. Therefore, it could be said that the all the NCMO samples were crystallized out with anti fluorite structural form of CeO_2, which is similar with the results that had been reported by Tang et al. [17]. Tang et al. [17] suggested that the crystallization nature of cerium–manganese mixed oxide is dependent on the Mn/(Mn + Ce) atomic ratio. When the Mn/(Mn + Ce) ratio is greater than 0.75, the mixed oxide should crystallize as Mn_2O_3 [17]. The EDS analysis for the NCMO-1b sample showed that the Mn/(Mn + Ce) < 0.4, indicating the number of cerium atoms were greater than that of manganese atoms. Therefore, the mixed oxide was crystallized out with anti-fluorite structure of the CeO_2. Increase of the calcination temperature from (373 to 773) K did developed neither new phase nor segregation of the mixed oxide. This clearly indicated that the NCMO-1 sample was stable in that temperature range. Thus, the XRD peak patterns analysis suggested that the cerium–manganese mixed oxide had crystallized as antifluorite structure with nano-crystallite particles. Cerium and manganese present in all the NCMO samples are in +4 and +3 oxidation states respectively. Despite the existence of cerium (IV) ion is clearly identified from the XRD curves, the existence of manganese (III) ion is not clearly identified since the peaks are not appeared in the XRD patterns of NCMO samples. The reason behind this fact has been discussed previously, but according to our synthetic strategy the manganese ion present in the NCMO samples should be in the +3 oxidation state since this oxidation state is thermodynamically stable under the synthetic conditions of the samples.

Again, it had been aimed that the NCMO material will be applied for scavenging the undesired solutes from the contaminated water. Thus, the samples were investigated for their efficiencies of arsenic(V) sorption from the aqueous solutions at $pH_i = 7.0$, $I = 0.01$ M and $T = 303$ (± 1) K. It was found that the percentages of arsenic(V) removed from the solution of $C_0 = 5.0$ mg L^{-1} were >98.0, 97.5, 61.0 and 58.5, respectively, by NCMO-1a, NCMO-1b, NCMO-1c and NCMO-2. It had revealed that NCMO-1a and NCMO-1b samples were equally efficient and better than the other two samples for removal of arsenic(V) from the aqueous solutions. Again, analysis of the manganese concentration in filtered solutions after batch sorption study showed that the concentrations (mg L^{-1}) of manganese in tested solutions were 0.13 and <0.05 from the samples NCMO-1a and NCMO-1b, respectively. It indicated that the manganese leached out from the surface of NCMO-1a sample was 2.5 times greater than that from the surface of NCMO-1b sample. Thus, the NCMO-1b sample was investigated for the further characterization with the NCMO-2 sample and, NCMO-1b was used for the investigations of arsenic(V)-sorption from aqueous solutions.

3.3. AFM analysis

The AFM images for topography of NCMO samples are shown in Figs. S1a–S3b. It was found from the distribution curves of particle size (Figs. S1d and S2b) that the average sizes (nm) of particles in NCMO-1a and NCMO-1b samples were ranged in 50–60 and 140–150, respectively. However, the particle size of NCMO-1c sample was so big that the distribution of particle size could not be detected individually. This had suggested that the particles in NCMO samples went to agglomeration/copolymerization with the increase of incinerating temperature, indicating the increase of particles size.

Three particles of the NCMO-1a sample were captured, and estimated their size, which are shown in Fig. S1c. It was found that the length of each particle was close to 370 nm, and the height was ranged between 10 and 20 nm. It was found from Fig. S2c that the particle of NCMO-1b which was captured under the microscope had the length almost 1100 nm with approximate height 170 nm. This indicated that the particle size was increased with increasing incineration temperature. The results found were similar with that reported by Theocharis et al. [18]. According to them [18], the size of the particles was initially 5.0 nm, which had increased to 63.6 nm after incineration at high temperature. The particle size, however, for the NCMO-1c sample was detected to be largest, presumably the particle agglomerations were not ruptured to smaller units for lacking of proper sonication. Consequently, the individual particles could not be captured under the AFM for analysis (Fig. S3a). Fig. S3b shows that the particles of NCMO-1c were also too large (>900 nm), which could be observed as a chain (encircled, Fig. S3b).

3.4. TEM analysis

The TEM images of NCMO-1b and NCMO-2 samples are shown in Fig. 2A and B, respectively. It was found that the NCMO-1b was agglomeration of spherical particles of size ranged in 70–90 nm, which appeared as the garland like chain (Fig. 2A) showing the presence of void space. It was also found that the dimension of NCMO-1b particles was greater than that was reported by Liwei et al. [26]. The TEM image of NCMO-2 (Fig. 2B) had shown with two different magnifications. It had been seen that the average particle size was ranged in (15–20) nm. The fingerprint like appearance in the TEM image (Fig. 2B) of NCMO-2 at higher magnification suggested that the material (NCMO-2) was highly crystalline. As the cerium oxide and manganese oxide particles present in the mixed oxide did not posses different shapes, it had been impossible to specify them individually in the TEM pictures.

3.5. SEM analysis

The SEM images of NCMO-1b and NCMO-2 samples are shown in Fig. 3A. It was found from the image of NCMO-1b sample (image-a, Fig. 3A) that the particles were inter connected in a sheet like structure, and that had been more clearly visible from the image-b in Fig. 3A. The sheet might be the layered cerium oxide onto which the manganese oxide particles were attached. The black spots appeared in the images were the void spaces on oxide surface. Again, the dispersion of manganese oxide particles on ceria matrix was suggested from the SEM pictures. The mole ratio of Ce:Mn was found to be 1:1, which had been obtained from the EDS spectrum (Fig. 3B) of NCMO-1b sample. The SEM image of NCMO-2 (image-c, Fig. 3A) showed that the material had high degree of crystalline phases

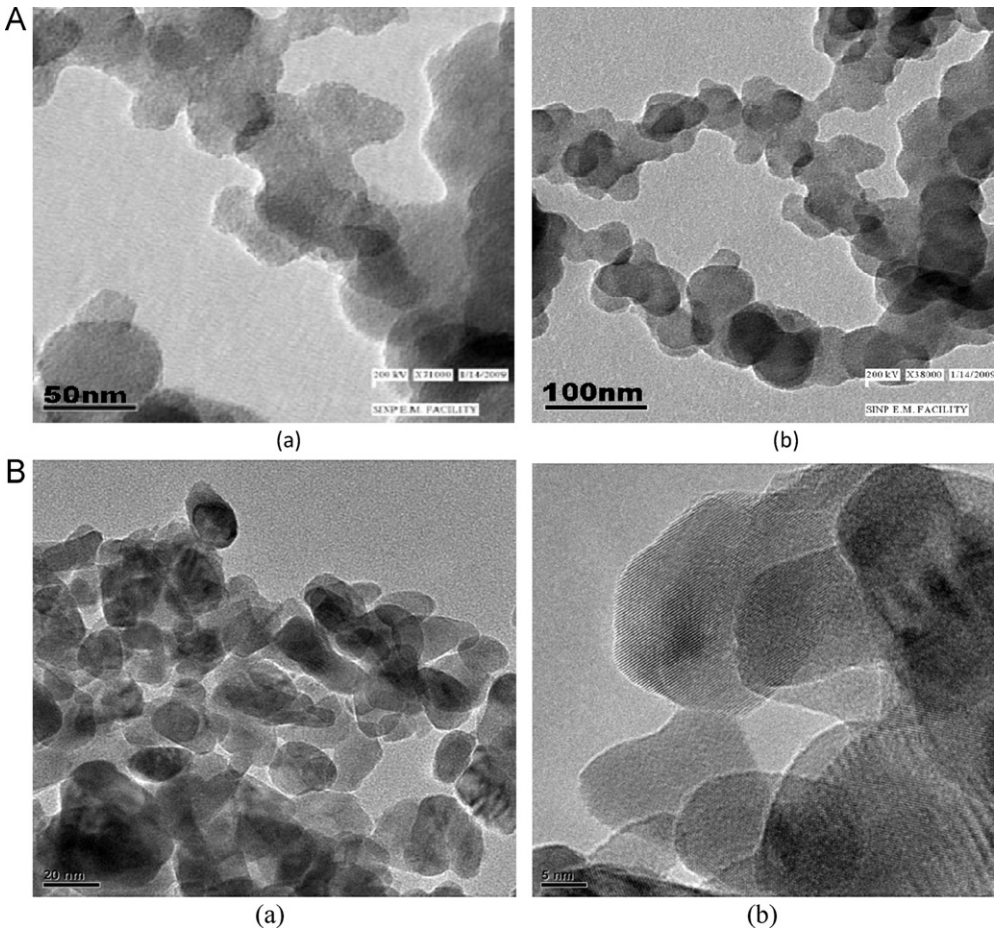

Fig. 2. (A) Transmission electron microscopic (TEM) image of NCMO-1b. (a) 50 nm scale (b) 100 nm scale (Adobe Photoshop scanned figure). (B) Transmission electron microscopic (TEM) image of NCMO-2. (a) 20 nm scale (b) 5 nm scale.

without any definite surface morphology. Thus, it could be said that both NCMO-1b and NCMO-2 samples had no regular surface morphology.

3.6. BET surface area analysis

The BET surface area was analyzed for only NCMO-1b sample (Fig. S4a), because the pre-screening based on the arsenic(V) sorption efficiency at pH 7.0 (±0.1) and $T = 303$ K and solubility tests of as-prepared four samples indicated that the NCMO-1b sample should be only the optimal material. Analyzed BET specific surface area for NCMO-1b sample was quite high (116.96 $m^2\ g^{-1}$), and that was found to be higher than the cerium oxide nano particles [30] and cerium–manganese mixed oxide [19]. Fig. S4b shows the pore size distribution in NCMO-1b sample. Pore size and volume estimated were 9.42 nm and 0.25 $cm^3\ g^{-1}$, respectively, indicating micro porosity of NCMO-1b material.

3.7. FTIR analysis

Fig. 4A shows the FTIR spectra of NCMO-1b (spectrum-a), manganese oxide (spectrum-b) and cerium oxide (spectrum-c) samples. Absorption bands centered at wave number (ν, cm^{-1}) 510 and 451 in spectrum-b were normal stretching and bending modes of the Mn–O bond, which disappeared in spectrum-a (inset, Fig. 4A). The FTIR spectra of cerium oxide, manganese oxide and NCMO-1b samples in the range of $\nu = 1000$–$400\ cm^{-1}$ are shown in the inset of Fig. 4A. It showed a sharp band at $\nu = 670\ cm^{-1}$ in spectrum-a for the NCMO-1b sample, which was found to be absent in the other two spectra. However, the full-scale view of the spectrum-a (NCMO-1b) showed a broad band at $\nu \sim 450\ cm^{-1}$, which are collections of some low bands in the modified scale of the spectrum. These bands were absent in the spectra of two pure oxides (inset of Fig. 4A). The synthesis of the oxide sample was so designed that the $(Mn)_{at}/(Ce)_{at} = 1$ in NCMO-1b and the EDS analysis showed that ratio was less than 1. The manganese atoms in NCMO samples may not form bond with all the cerium atoms. But, it is definite that some interactions took place between cerium and manganese atoms because the broad bands of manganese oxide disappeared almost in the spectrum-a (NCMO-1b). Fig. 4B shows the FTIR spectra of samples NCMO-1b (spectrum-a), physical mixtures of cerium oxide and manganese oxide that made by simple mixing at three different mole proportions (1:1, 1:2 and 2:1) (spectra-b–d), and NCMO-2 (spectrum-e). The FTIR bands appeared for the physical mixtures were at $\nu \sim 620$ and $500\ cm^{-1}$ (spectra-b–d), which were absent in spectrum-a (NCMO-1b). The other bands of the physical mixtures and NCMO-1b were almost at similar ν values, which were the bending and stretching modes of vibration of O–H bond. Thus, there are no direct interactions between the two oxides in the physical mixtures, and the characteristics bands of each oxide appeared. However, the band positions were changed to some small extent in NCMO samples. This proved that the sample (NCMO-1b) was not a simple physical mixture of the pure oxides. The FTIR spectrum-e of NCMO-2 (Fig. 4B) showed no characteristic bands for the O–H stretching and bending modes of vibrations, indicating the absence of hydroxyl group. This indicated the poor arsenic(V) scavenging capacity of NCMO-2 from the aquatic phases.

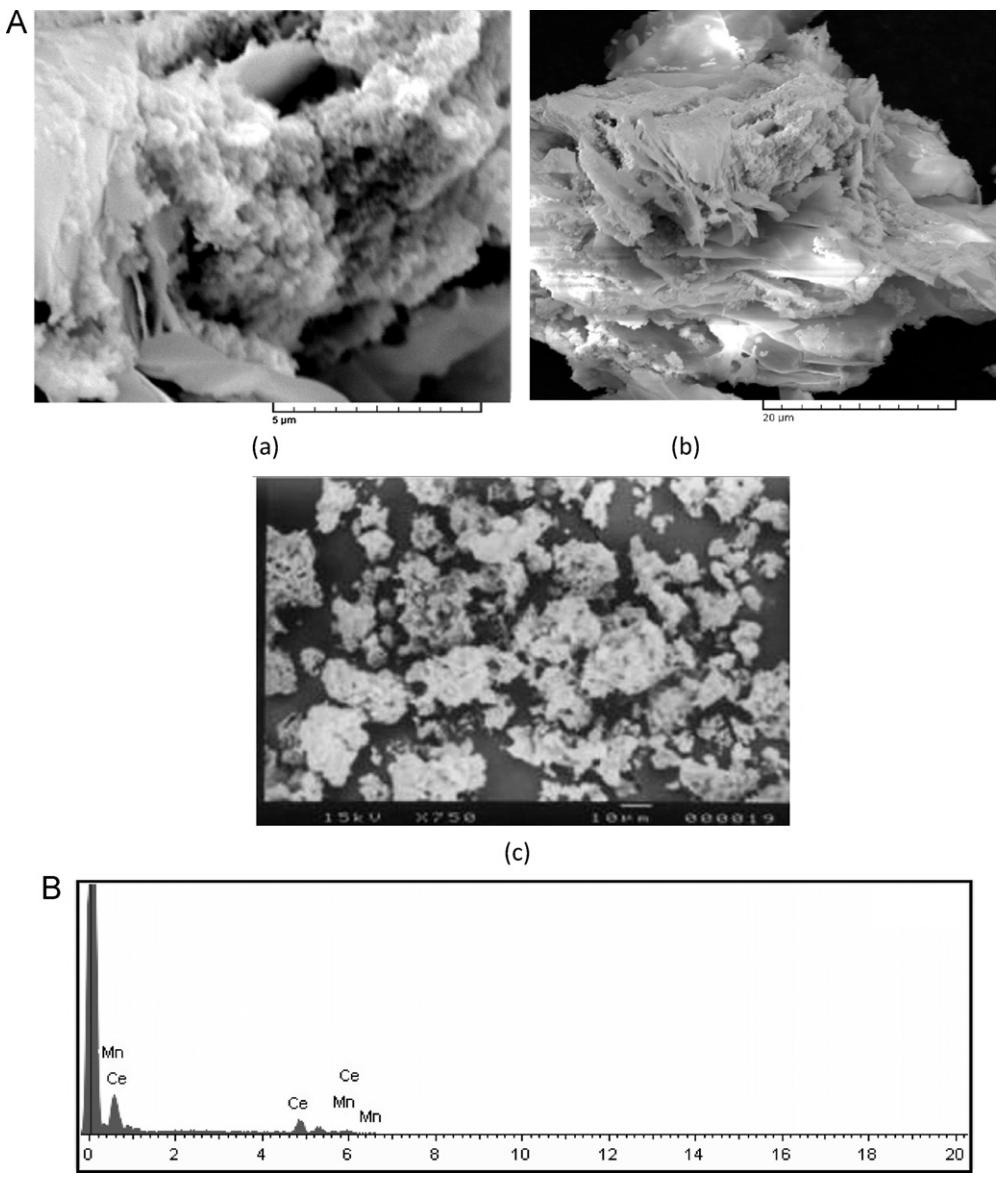

Fig. 3. (A) Scanning electron micrograph of (a) NCMO-1b (5 μm scale), (b) NCMO-1b (10 μm scale), and (c) NCMO-2. (B) EDS analysis of NCMO-1b for the surface composition.

3.8. Raman spectra analysis

Fig. 4C shows the Raman spectrum of the NCMO-1b sample. Literature showed [20] that the fluorite structure of pure ceria showed a strong band centered at ν ~462–466 cm^{-1} due to the F_{2g} active mode with a very small component at ν ~590 cm^{-1}, which was due to the non degenerate Raman inactive LO (Linear Oscillation) mode [15]. However, the NCMO-1b showed a band centered at ν = 460 cm^{-1}, which was found to be almost symmetric in nature. Raman shift was not so strong compared to the pure ceria which was contrary to the earlier finding by Arena et al. [20]. This observation indicated clearly that the Ce–O bond became weak to a small extent in the NCMO-1b sample compared to that of pure ceria. Low absorption band centered at ν ~643 cm^{-1} was due to the symmetric vibration of Mn–O bond, indicating the presence of manganese oxide in NCMO-1b sample.

3.9. pH_{ZPC} analysis

As the aim of the present work was synthesis of potential adsorbent for filtering undesired solutes from the contaminated water; the analysis of pH for the zero surface charge (pH_{ZPC}) of materials is justifiable. Thus, the pH_{ZPC} of NCMO-1b sample was estimated by pH titration method [31] in 0.01 M NaCl solution (Fig. S5), and that was found to be 6.5 (±0.1). The value (6.5 ± 0.1) indicated that the surface of the oxide particles should be positive at pH <6.5 and negative at pH >6.5, which indicated the sorption possibility of $(HO)_2As^VO^-$ or $(HO)As^VO_2^{2-}$ species via Columbic forces at pH ~7.0.

3.10. pH effect on arsenic(V) sorption

Fig. 5 shows the change of sorption percentage of arsenic(V) on NCMO-1b with increasing pH_i. It was found that the sorption percentages of arsenic(V) were nearly constant up to the pH_i 6.0, and decreased slightly from pH_i 6.0 to 8.0. The decrease of arsenic(V) sorption was high at pH_i above 8.0. When the solution pHi increased from 8.0 to 11.0, the sorption percentages of arsenic(V) reduced from 80.0 (±2.0) to 45.0 (±5.0) and, can be explained by the pH_{ZPC} value (6.5) of NCMO-1b. The positive surface of NCMO-1b binds the $H_2AsO_4^-$ or $HAsO_4^{2-}$ with Columbic forces strongly up to the pH_i <6.5 (pH_{ZPC}). This had explained the high removal percentage

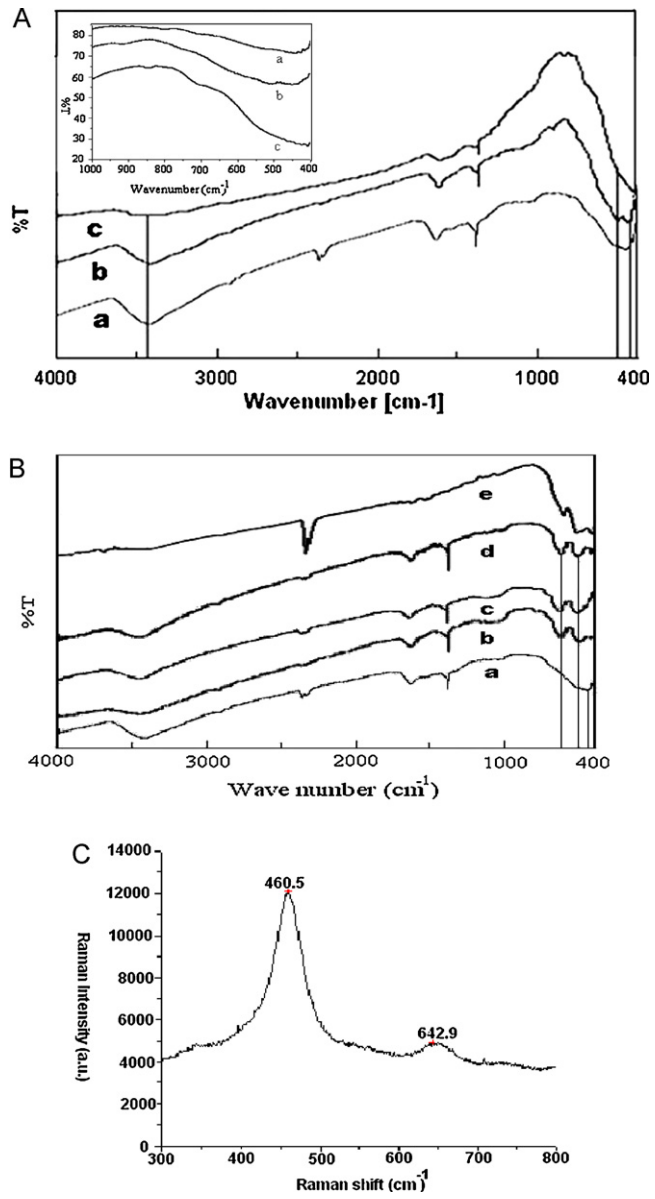

Fig. 4. (A) FTIR spectra of (a) NCMO-1b, (b) pure manganese oxide, and (c) pure cerium oxide. (B) FTIR spectra of (a) NCMO-1b, physical mixture of cerium oxide and manganese oxide (b) 1:1, (c) 1:2, (d) 2:1, and (c) NCMO-2. (C) Raman spectra of NCMO-1b.

of arsenic(V) in acid pH-range. With enhancing pH_i from 6.5, the surfaces of NCMO-1b should transform to negative, and repel the $H_2AsO_4^-$ or $HAsO_4^{2-}$ species for likeness of charges. This had given the account for of less removal percentage of arsenic(V) at $pH_i \geq 8.0$. The effect of pH on the removal of arsenic(V) noted herein was found to be identical with that reported by Lakshmipathiraj et al. [32].

3.11. Kinetic study

Fig. 6 shows the time dependent sorption amount (q_t, mg g^{-1}) of arsenic(V) by NCMO-1b with increasing time for reaction at pH_i 7.0 (±0.1), $I = 0.01$ M and $T = 303$ (±1.0) K. It had indicated that the time required to reach equilibrium was about 30 min. Rapid uptake of arsenic(V) was noted at the initial 20 min, and that reduced with increasing time of contact; which is due to the reduction of accessible sorption sites and Columbic inhibition between the species that already sorbed and the species at interface for sorption. The kinetic

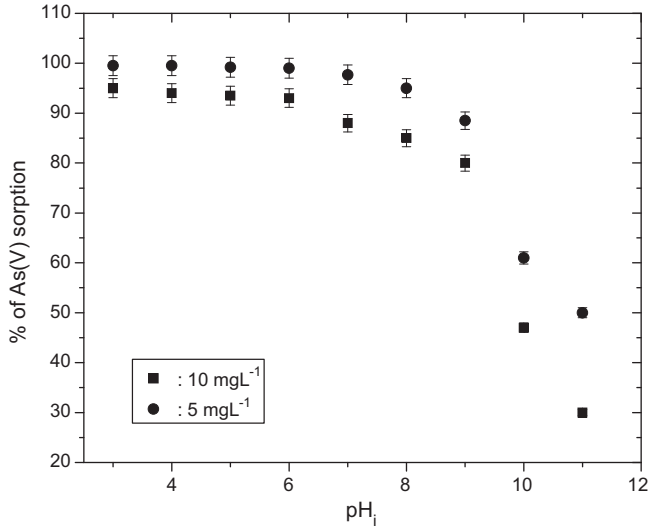

Fig. 5. The plots of sorption percentage of As (V) by NCMO-1b versus pH_i. ($T = 303 \pm 1.6$ K, $I = 0.01$ M).

data for the present reaction were analyzed by the pseudo first order (Eq. (1)) [33] and the pseudo second order model equations (Eq. (2)) [34].

$$\log(q_e - q_t) = \log\ q_e - \frac{(k_1 t)}{2.303} \quad (1)$$

$$\frac{t}{q_t} = \frac{1}{k_2 \cdot q_{t^2}} + \frac{k_2}{q_e} \quad (2)$$

where q_e and q_t are the sorption amount (mg g^{-1}) of arsenic(V) at equilibrium and at time, t (min), respectively; and k_1 (min^{-1}) and k_2 (g mg^{-1} min^{-1}) are the rate constants for the respective Eqs. (1) and (2).

The kinetic parameters were estimated from the non-linear analysis of the data (Fig. 6) using Eqs. (1) and (2) and the values are summarized in Table 1. The R^2 and χ^2 values (Table 1) indicated that the reaction kinetics for arsenic(V) sorption by NCMO-1b described the pseudo second order model very well under the conditions of present reaction. The k_2 values (Table 1) showed that the arsenic(V) sorption on NCMO-1b took place rapidly at the lower concentration

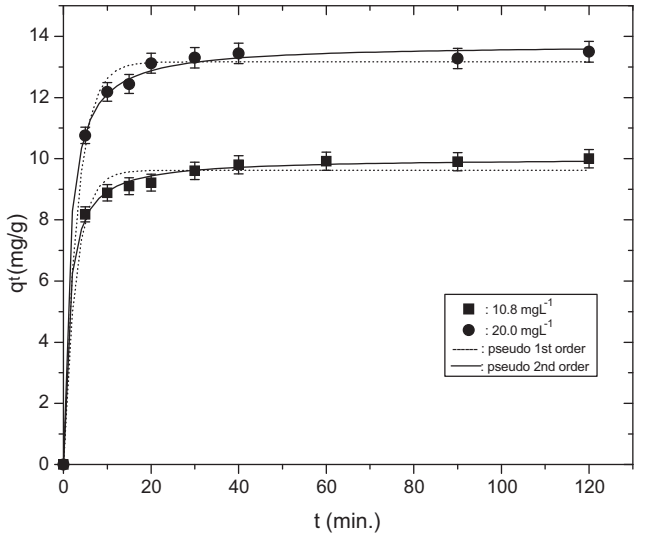

Fig. 6. The plots of time dependent sorption capacity (q_t, mg g^{-1}) of As (V) by NCMO-1b versus reaction time (t, min) at $T = (303 \pm 1.6)$ K, $pH_i = (7.0 \pm 0.2)$ and $I = 0.01$ M (—) Pseudo second order and (. . .) pseudo first order kinetic fits.

Table 1
Kinetic model parameters evaluated for the sorption of arsenic(V) on NCMO-1b at $pH_i = (7.0 \pm 0.1)$, $I = 0.01$ M and $T = 303 \pm 1.0$ K.

Arsenic(V) concentration ($mg\,L^{-1}$)	Pseudo-first order parameters				Pseudo-second order parameters			
	k_1 (min^{-1})	q_e ($mg\,g^{-1}$)	R^2	χ^2	k_2 ($g\,mg\,min^{-1}$)	q_e ($mg\,g^{-1}$)	R^2	χ^2
10.8	0.354 (±0.044)	9.617 (±0.130)	0.988	0.122	0.082 (±0.007)	10.012 (±0.063)	0.999	0.015
20.0	0.320 (±0.027)	13.165 (±0.143)	0.994	0.124	0.055 (±0.005)	13.738 (±0.100)	0.999	0.031

Table 2
The isotherm parameters estimated by the non-linear analysis of equilibrium arsenic(V) sorption data on NCMO-1b at $pH_i = (7.0 \pm 0.1)$, $I = 0.01$ M and $T = 303 \pm 1.0$ K.

Isotherm parameters							
Langmuir				Freundlich			
q_m ($mg\,g^{-1}$)	K_a ($L\,g^{-1}$)	R^2	χ^2	n	K_F ($mg\,g^{-1}$)	R^2	χ^2
18.653 (±1.718)	0.555 (±0.264)	0.803	4.998	4.611 (±0.295)	9.020 (±0.334)	0.986	0.348

($10.8\,mg\,L^{-1}$) than the higher one ($20\,mg\,L^{-1}$). Thus, it is suggested that NCMO-1b could be an efficient material to remove arsenic(V) from the contaminated groundwater.

3.12. Isotherm study

Fig. 7 demonstrates the equilibrium capacity (q_e, $mg\,g^{-1}$) of arsenic(V) sorption of NCMO-1b at $pH_i = 7.0$ (±0.1), $I = 0.01$ M and $T = 303$ (±1.0) versus equilibrium arsenic(V) concentrations, (C_e, $mg\,L^{-1}$). The equilibrium data (Fig. 7) were fitted to the Langmuir (Eq. (3)) and the Freundlich (Eq. (4)) isotherm models, which are usually used to describe the equilibrium sorption data [35].

$$\text{Langmuir equation}: q_e = \frac{q_m K_a C_e}{1 + K_a C_e} \quad (3)$$

$$\text{Freundlich equation}: q_e = K_F C_e^{(1/n)} \quad (4)$$

where q_m and K_a are the Langmuir constants related to monolayer sorption capacity ($mg\,g^{-1}$) and sorption equilibrium constant ($L\,g^{-1}$), respectively. K_F and n are the Freundlich constants related to the sorption capacity ($mg\,g^{-1}$) and sorption intensity, respectively.

Non-linear analysis of q_e versus C_e data using model Eqs. (3) and (4) was used to estimate the related isotherm parameters and the values are presented in Table 2. Based on either the statistical error chi square (χ^2) or the linear regression co-efficient (R^2) values, it can be said that the equilibrium data (Fig. 7) described the Freundlich equation (4) very well ($\chi^2 = 0.35$, $R^2 = 0.99$), and far better than the Langmuir equation (3) ($\chi^2 = 5.00$, $R^2 = 0.80$). This has indicated that the sorption sites on NCMO-1b surface were heterogeneous, and not equally accessible by the solutes. Similar type of observation was reported for the arsenate adsorption on ceria nanoparticles supported on carbon nanotubes [36]. The monolayer sorption capacity (q_m) estimated was $18.65\,mg\,g^{-1}$ at working pH and other specified reaction conditions, indicating good scope of applicability of this material for high arsenic water treatment. The estimated q_m value was compared with that of some other reported materials (Table 3). It. revealed that NCMO-1b could be an efficient material for the arsenic(V) removal from water, despite the efficiency comparison with other materials is somewhat difficult for difference of the used experimental conditions. However, it can be said that NCMO-1b is a better material for scavenging arsenic(V) than many others excepting ferrihydrite [37] and activated carbon [43].

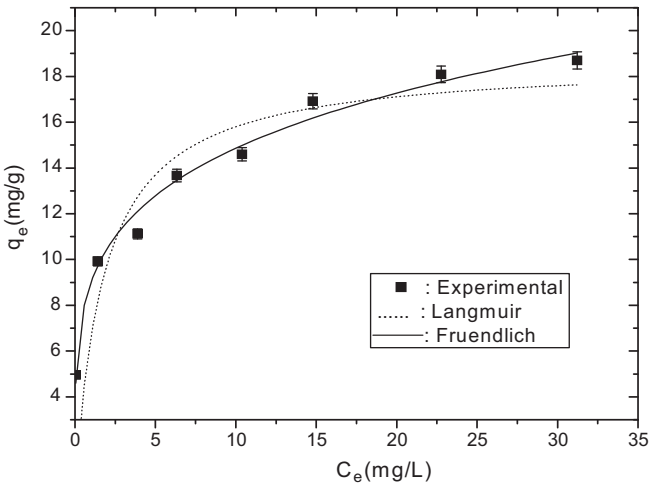

Fig. 7. The plot of q_e ($mg\,g^{-1}$) versus C_e ($mg\,L^{-1}$) on As (V) sorption by NCMO-1b at $T = 303$ (±1.6) K, $pH_i = 7.0$ (±0.2) and I = 0.01 M with Fruendlich (—) and Langmuir (- - -) models fit of the data.

3.13. Energy of sorption

The equilibrium data shown in Fig. 7 were analyzed by the Dubinin–Radushkevich (D–R) isotherm equation (5) [44] for the estimation of sorption energy.

$$Q_e = Q_m \exp(-K_{DR}\varepsilon^2) \quad (5)$$

where Q_e and Q_m are the equilibrium and saturated sorption capacities ($mol\,kg^{-1}$), respectively, and K_{DR}, a constant related to the

Table 3
Comparison of the Langmuir monolayer arsenic(V) sorption capacity (q_m, $mg\,g^{-1}$) with some reported sorbent materials.

Adsorbent	pH	Concentration range ($mg\,L^{-1}$)	Adsorption capacity ($mg\,g^{-1}$)	Reference
Ferrihydrite	7.0	0–150	68.75	[36]
MnO_2 (MOI)	7.9	<1	0.172	[37]
Akaganite-type nanocrystal	7.5	5–20	1.80	[38]
Mixed rare earth oxide	6.5	50	2.950	[39]
Activated alumina	5.2	2.85–11.5	15.90	[40]
Granular ferricoxide	8–9	5–100	8.50	[41]
Activated carbon	6.4–7.5	157–737	30.48	[42]
NCMO	7.0	5–40	18.653	Present work

Table 4
Thermodynamic parameters evaluated for the arsenic(V) sorption reaction with NCMO-1b at $pH_i = (7.0 \pm 0.1)$, $I = 0.01$ M.

Arsenic(V) concentration ($mg\,L^{-1}$)	ΔH° ($kJ\,mol^{-1}$)	ΔS° ($kJ\,mol^{-1}\,K^{-1}$)	ΔG° ($kJ\,mol^{-1}$)				
			283 K	293 K	303 K	313 K	323 K
5.0	+23.901	0.175	25.737	27.491	29.245	30.999	32.753

free energy ($mol^2\,kJ^{-2}$) of sorption, ε is the Polanyi potential and expressed by Eq. (6) below

$$e = RT \ln \left\{1 + \left(\frac{1}{C'_e}\right)\right\} \quad (6)$$

where C'_e ($mol\,L^{-1}$) has usual meaning with C_e; R and T, respectively, are the molar gas constant ($kJ\,mol^{-1}$) and absolute temperature (K). The values of Q_m and K_{DR} were estimated from the plot of Q_e versus ε^2 (plot not shown). It was found that the present data described the D–R equation very well ($R^2 = 0.97$). The values of Q_m and K_{DR} estimated were 0.48 $mol\,kg^{-1}$ and $(1.7 \pm 0.2) \times 10^{-3}$ $mol^2\,kJ^{-2}$, respectively. The Eq. (7) relates the mean free energy (E, $kJ\,mol^{-1}$) of sorption with K_{DR}.

$$E = (-2K_{DR})^{-0.5} \quad (7)$$

It is known that if the value of E is ranged between 8.0 and 16.0 $kJ\,mol^{-1}$, the sorption should be ion-exchange type. The value of E for the present sorption reaction was calculated to be 17.15 $kJ.\,mol^{-1}$, which is greater than 16.0 $kJ.\,mol^{-1}$. Thus, the arsenic(V) sorption by NCMO-1b was chemisorbed by NCMO-1b.

3.14. Thermodynamic parameters

Thermodynamic parameters viz the changes of Gibbs free energy (ΔG°), enthalpy (ΔH°) and entropy (ΔS°) were analyzed using the standard relations available in literature [45]. Values of the thermodynamic parameters estimated from the plot of $\ln C_s/C_L$ versus $1/T$ (Fig. S6) are shown in Table 4. It had been seen that the ΔG° values were ranged in (−25.74 to −32.75) $kJ\,mol^{-1}$ in the range of $T = (283–323)$ K. This indicated that the spontaneous nature of the reaction increased with increasing temperature. Endothermic nature of the sorption reaction could be realized from the positive ΔH° (+23.90 $kJ\,mol^{-1}$) value. Again, the increase of entropy (ΔS° = +0.18 $kJ\,mol^{-1}\,K^{-1}$) for the sorption reaction suggested that the randomness increased at solid–liquid interface in this reaction, which is similar with the results that was reported by Banerjee et al. [45].

3.15. Effect of some other anions

The effect of phosphate, sulfate and bicarbonate ions on arsenic(V) sorption ($C_0 = 5.0\,mg\,L^{-1}$) by NCMO-1b was assessed with incorporation of three different concentrations of each ions at $pH_i = 7.0$ (±0.2), and the percentage of arsenic(V) sorption obtained was plotted against the concentration of (other anion/arsenic(V)) (Fig. S7a–c). It had been seen from Figs. S7b and S7c that sulfate and bicarbonate had no notable adverse effect, while the phosphate ion had strong adverse effect on the arsenic(V) removal by NCMO-1b (Fig. S7a). It had been found that the percentage of arsenic(V) sorption decreased from 97.7 (±1.5) to 68.8 (±1.2) when ratios of the molar concentration of phosphate to arsenate increased from 0 to 2. This adverse effect may be attributed to preferential/selective sorption of phosphate ion by the NCMO-1b surface competing with arsenate in solution at $pH_i = 7.0$ (±0.2) because of the similar chemistry of phosphate and arsenate.

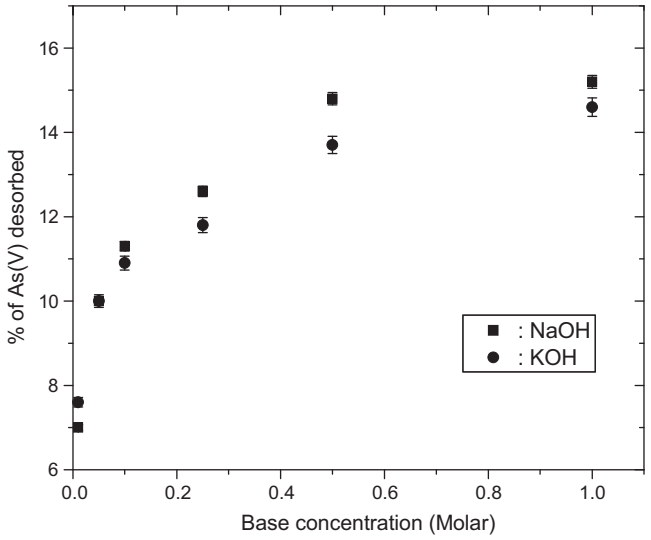

Fig. 8. Desorption of arsenic(V) from arsenic(V) loaded NCMO-1b surface.

3.16. Desorption study

Fig. 8 shows the results on arsenic(V) desorption with NaOH and KOH solutions. It was found that the percentages of arsenic(V) desorption increased gradually with increasing molar concentration of the used alkalis, and remained nearly constant at above 0.5 M alkali concentration. The percentage of arsenic(V) desorption obtained from the solid surface was ~15–16% even when the concentration of alkali solution increased to 1.0 M. This is presumably due to the strong binding force between the solid surface and arsenic(V) species ($H_2AsO_4^-$), indicating chemical binding of the solute with NCMO-1b.

3.17. TCLP Test of As^V-NCMO-1b

According to the U.S. EPA, [28], if the leached arsenic concentration from the contaminated solid waste is $\geq 5.0\,mg\,L^{-1}$, the solid waste should be marked as the hazardous waste, and that should need special precaution for disposal of the waste material. The results on the TCLP test of As^V-NCMO-1b sample (27.98 $mg\,As\,g^{-1}$) showed that the leached arsenic concentration in the used fluid (acetate buffer, $pH = 4.93 \pm 0.05$) was found to be 0.02 (±0.01) $mg\,L^{-1}$, which is about 200 times lower than the U.S. EPA specified limit [28]. Thus, the arsenic-rich solid could be marked as non-hazardous material and that can be disposed off safely in the surface landfill.

3.18. Arsenic(V) sorption mechanism

Fig. 9A shows the FTIR spectra of NCMO-1b (spectrum-a) and As^V-NCMO-1b (spectrum-b). The band appeared at 802 cm^{-1} in spectrum-b was for the As–O bond indicating the presence of arsenic(V) species on NCMO-1b surface. The peak intensity of both O–H stretching and bending modes of vibration increased slightly

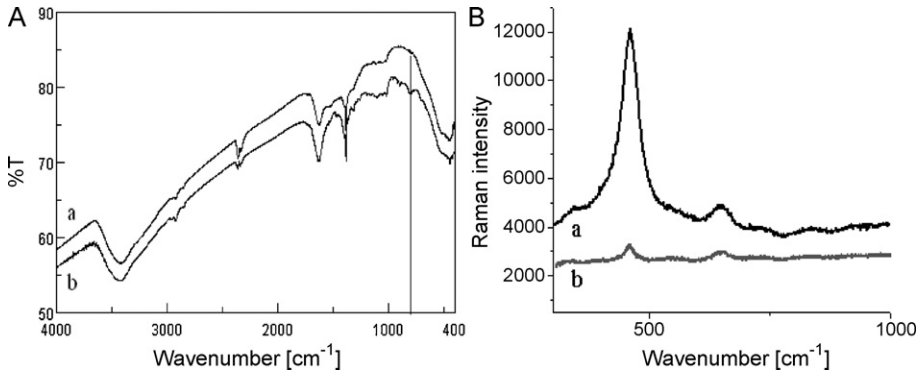

Fig. 9. (A) FTIR spectra of (a) NCMO-1b (b) As (V) loaded NCMO-1b and (B) Raman spectra of (a) NCMO-1b and (b) As (V) loaded NCMO-1b.

with arsenic(V) sorption by NCMO-1b, which is due to the replacement of one surface –OH group by one $-H_2AsO_4^-$ species that has two –OH groups. Replacement of surface –OH groups by arsenic(V) species was observed more clearly when Raman spectra of the materials were taken (Fig. 9B). It had been seen that the peaks at around 460 and 663 cm^{-1} in the Raman spectra of NCMO-1b were almost disappeared with arsenic(V) sorption. The M–OH bonds in NCMO-1b sample had been replaced by $M–O–As^V$ bonds and, thus the arsenic(V) sorption by NCMO-1b was of chemisorptions type. High sorption energy (17.15 kJ mol^{-1}) estimated from the D–R isotherm analysis of equilibrium data and low percentages of arsenic(V) desorption (15–16%) from the oxide surface had supported the chemisorptions nature of arsenic(V) by NCMO-1b. Thus, the sorption reaction could be presented by the reaction below:

$$M–OH + H_2AsO_4^- \rightarrow M–OAsO(OH)_2 + OH^-$$

4. Conclusion

The synthesis of nano structured cerium associated manganese oxide (NCMO) by redox conversion co-precipitation and sol–gel methods showed that the dimension of material particles was greater for the former method than the later. The crystalline phases in the as-prepared materials were good with irregular surface morphology. Incineration of NCMO-1 sample with increasing temperature increased the particle dimension. The materials when used for the arsenic(V) removal at neutral pH and room temperature showed that the sample NCMO-1b had good efficiency of arsenic removal. The microcrystalline material (NCMO-1b) was porous and nanoparticles (80–90 nm) agglomerate with surface Ce:Mn ~ 1:1. High BET surface area of NCMO-1b supported the presence of nanoparticle in the material. This material could remove ~98% of arsenic(V) at pH_i = 3.0–7.0 from the tested solutions at room temperature. The arsenic(V) sorption by NCMO-1b at pH = (7.0 ± 0.2), I = 0.01 M and T = (303 ± 1.6) K took place obeying the pseudo second order kinetics. Well fit of equilibrium data with the Freundlich isotherm model indicated the heterogeneity of NCMO-1b surface. The sorption reaction was endothermic and spontaneous, which took place with increasing entropy. The chemically similar phosphate ion showed negative influence on the arsenic(V) sorption by NCMO-1b. Low desorption percentages of arsenic(V) (15–16%), high mean sorption energy (17 kJ mol^{-1}) and the FTIR analyses suggested that the sorption reaction was chemisorption type.

Acknowledgements

Authors are gratefully acknowledged the Head, Department of Chemistry and the Vice-Chancellor, Presidency University (formerly Presidency College), Kolkata, India for the laboratory facilities.

Appendix A. Supplementary data

Supplementary data associated with this article can be found, in the online version, at doi:10.1016/j.cej.2011.05.092.

References

[1] W.X. Zhang, Nano-scale iron particles for environmental remediation: an overview, J. Nanopart. Res. 5 (2003) 323–332.
[2] A.V. Murugan, A.B. Gaikward, V. Samuel, V. Ravi, Ceram. Int. 33 (2007) 569.
[3] H. Liu, C. Hu, Z.L. Wang, Composite-hydroxide-mediated approach for the synthesis of nanostructures of complex functional-oxides, Nano Lett. 6 (2006) 1535–1540.
[4] M.H. Khedr, A.A. Omar, S.A. Abdel-Moaty, Magnetic nanocomposites: preparation and characterization of Co-ferrite nanoparticles, Colloids Surf. A: Physicochem. Eng. Aspects 281 (2006) 8–14.
[5] J.H. Meng, G. Yang, L. Yan, X.Y. Wang, Synthesis and characterization of magnetic nanometer pigment Fe_3O_4, Dyes Pigments 66 (2005) 109–113.
[6] Q. Song, Z. Zhang, Shape control and associated magnetic properties of spinel cobalt ferrite nanocrystals, J. Am. Chem. Soc. 126 (2004) 6164–6168.
[7] Y. Zhang, M. Yang, X.M. Don, Arsenate adsorption on an Fe–Ce bimetal oxide adsorbent: role of surface properties, Environ. Sci. Technol. 39 (2005) 7246–7253.
[8] E. Deschamps, V.S.T. Ciminelli, W.H. Holl, Removal of As(III) and As(V) from Water using a natural Fe-MN enriched sample, Water Res. 39 (2005) 5212–5220.
[9] S. Zhang, H. Niu, Y. Cai, X. Zhao, Y. Shia, Arsenite and arsenate adsorption on coprecipitated bimetal oxide nanomaterials: $MnFe_2O_4$ and $CoFe_2O_4$, Chem. Eng. J. 158 (2010) 599–607.
[10] G. Zhang, J.H. Qu, R.R. Liu, G.T. Li, Removal mechanism of as by a novel Fe–Mn binary oxide adsorbent: oxidation and sorption, Environ. Sci. Technol. 41 (2007) 4613–4619.
[11] K. Gupta, A. Maity, U.C. Ghosh, Manganese associated nanoparticles agglomerate of iron(III) oxide: synthesis, characterization and arsenic(III) sorption behavior with mechanism, J. Hazard. Mater. 184 (2010) 832–842.
[12] K. Gupta, K. Biswas, U.C. Ghosh, Nanostructure iron(III)–zirconium(IV) binary mixed oxide: synthesis, characterization, and physicochemical aspects of arsenic(III) sorption from the aqueous solution, Ind. Eng. Chem. Res. 47 (2008) 9903–9912.
[13] K. Gupta, S. Saha, U.C. Ghosh, Synthesis and characterization of nanostructure hydrous iron–titanium binary mixed oxide for arsenic sorption, J. Nanopart. Res. 10 (2008) 1361–1368.
[14] T. Basu, K. Gupta, U.C. Ghosh, Equilibrium and thermodynamics on arsenic(III) sorption reaction in the presence of background ions occurring in groundwater with nanoparticle agglomerates of hydrous iron(III) + chromium(III) mixed oxide, J. Chem. Eng. Data 55 (2010) 2039–2047.
[15] R. Jothiramalingam, B. Viswanathan, T.K. Varadarajan, Preparation, characterization and catalytic properties of cerium incorporated porous manganese oxide OMS-2 catalysts, Catal. Commun. 6 (2005) 41–45.
[16] S Yasyerli, Cerium–manganese mixed oxides for high temperature H_2S removal and activity comparisons with V–Mn, Zn–Mn, Fe–Mn sorbents, Chem. Eng. Process. 47 (2008) 577–584.
[17] X. Tang, Y. Li, X. Huang, Y. Xu, H. Zhu, J. Wang, W. Shen, MnO_x–CeO_2 mixed oxide catalysts for complete oxidation of formaldehyde: effect of preparation method and calcination temperature, Appl. Catal. B: Environ. 62 (2006) 265–273.
[18] C.R. Theocharis, G. Kyriacou, M. Christophidou, Preparation and characterization of nanoporous ceria containing heteroatoms, with and without a matrix, Adsorption 11 (2005) 763–767.

[19] G. Zhou, P.R. Shah, R.J. Gorte, A study of cerium–manganese mixed oxides for oxidation catalysis, Catal. Lett. 120 (2008) 191–197.
[20] F. Arena, G. Trunfio, J. Negro, B. Fazio, L. Spadaro, Basic evidence of the molecular dispersion of MnCeOx catalysts synthesized via a novel "redox-precipitation" route, Chem. Mater. 19 (2007) 2269–2276.
[21] S. Hamoudi, F. Larachi, A. Adnot, A. Sayari, Characterization of spent MnO2/CeO2 wet oxidation catalyst by TPO–MS, XPS, and S-SIMS, J. Catal. 185 (1999) 333–344.
[22] M. Machida, M. Uto, D. Kurogi, T. Kijima, MnO_x-CeO_2 binary oxides for catalytic NOx sorption at low temperatures. Sorptive removal of NOx, Chem. Mater. 12 (2000) 3158–3164.
[23] B. Murugan, A.V. Ramaswamy, Nature of manganese species in $Ce_{1-x}Mn_xO_2$-δ solid solutions synthesized by the solution combustion route, Chem. Mater. 17 (2005) 3983–3993.
[24] H. Chen, A. Sayari, A. Adnot, F. Larachi, Composition-activity effects of Mn–Ce–O composites on phenol catalytic wet oxidation, Appl. Catal. B: Environ. 32 (2001) 195–204.
[25] S.T. Hussain, A. Sayari, F. Larachi, Enhancing the stability of Mn–Ce–O WETOX catalysts using potassium, Appl. Catal. B: Environ. 34 (2001) 1–9.
[26] J. Liwei, S. Meiqing, W. Jun, C. Xia, W. Jiaming, H. Zhichang, Redox behaviors and structural characteristics of Mn0.1Ce0.9Ox and Mn0.1Ce0.6Zr0.3Ox, J. Rare Earths 26 (2008) 523–527.
[27] L.S. Clesceri, A.E. Greenberg, A.D. Eaton (Eds.), Standard methods for the examination of water, waste water, AWWA, WEF, APHA, Washington DC, 1998.
[28] 40 Codes of Regulations; U.S. Environmental Protection Agency: Washington, DC, 1992, Part 261, 31.
[29] Y. Zhang, M. Yang, X.M. Don, Arsenate Adsorption on an Fe–Ce Bimetal Oxide Adsorbent: Role of Surface Properties, Environ. Sci. Technol. 39 (2005) 7246–7253.
[30] J. Hu, Y. Li, X. Zhou, M. Cai, Preparation and characterization of ceria nanoparticles using crystalline hydrate cerium propionate as precursor, Mater. Lett. 61 (2007) 4989–4992.
[31] M.B. Babic, M.J. Milonjic, B.V. Kaludierovic, Point of zero charge and intrinsic equilibrium constants of activated carbon cloth, Carbon 37 (1999) 477–481.
[32] P. Lakshmipathiraj, B.R.V. Narasimhan, S. Prabhakar, G. Bhaskar Raju, Adsorption of arsenate on synthetic goethite from aqueous solutions, J. Hazard. Mater. 136 (2006) 281–287.
[33] S. Lagergren, zur theorie dersogenannten adsorption gelosterstoffe, Kungliga SVenska Vetenskapsakademiens, Handlingar 24, 1898, pp. 1–39.
[34] Y.S. Ho, G.A. McKay, A comparison of chemisorption kinetic models applied to. 615 pollutant removal on various sorbents, Trans. I Chem. E (part B) 76 (1998) 332–340.
[35] D. Pohrel, T. Viraghavan, Arsenic removal from an aqueous solution by modified A. niger biomass: batch kinetic and isotherm studies, J. Hazard. Mater. 150 (2008) 818–825.
[36] X. Peng, Z. Luan, J. Ding, Z. Di, Y. Li, B. Tian, Ceria nanoparticles supported on carbon nanotubes for the removal of arsenate from water, Mater. Lett. 59 (2005) 399–403.
[37] B.J. Lafferty, R.H. Loeppert, Methyl arsenic adsorption and desorption behavior on iron oxides, Environ. Sci. Technol. 39 (2005) 2120–2127.
[38] S. Ouvrard, M.O. Simonnot, M. Sardin, Reactive behavior of natural manganese oxides toward the adsorption of phosphate and arsenate, Ind. Eng. Chem. Res. 41 (2002) 2785–2791.
[39] E.A. Deliyanni, D.N. Bakoyannakis, A.I. Zouboulis, K.A. Matis, Sorption of As(V) ions by akaganéite-type nanocrystals, Chemosphere 50 (2003) 155–163.
[40] A.M. Raichur, V. Penvekar, Removal of As(V) by adsorption onto mixed rare earth oxides, Sep. Sci. Technol. 37 (2002) 1095–1108.
[41] T.F. Lin, J.K. Wu, Adsorption of arsenite and arsenate within activated alumina grains: equilibrium and kinetics, Water Res. 35 (2001) 2049–2057.
[42] W. Driehaus, M. Jekel, U. Hilderbrandt, Granular ferric hydroxide—a new adsorbent for the removal of arsenic from natural water, J. Water Supply: Res. Technol.—AQUA 47 (1998) 30–35.
[43] J. Pattanayak, K. Mondal, S. Mathew, S.B. Lalvani, A parametric evaluation of the removal of As(V) and As(III) by carbon-based adsorbents, Carbon 38 (2000) 589–596.
[44] Y. Kim, C. Kim, I. Choi, S. Rengaraj, J. Yi, Arsenic Removal Using Mesoporous Alumina Prepared via a Templating Method, Environ. Sci. Technol. 38 (2004) 924–931.
[45] K. Banerjee, G.L. Amy, M. Prevost, S. Nour, M. Jekel, P.M. Gallagher, C.D. Blumenschein, Kinetic and thermodynamic aspects of adsorption of arsenic onto granular ferric hydroxide (GFH), Water Res. 42 (2008) 3371–3378.